

Fluxes of atmospheric muons underwater depending on the small- x gluon density

A Misaki¹, T S Sinegovskaya², S I Sinegovsky²
and N Takahashi³

¹ Waseda University, Okubo 3-4-1, Shinjuku-ku, Tokyo, 169-8555 Japan

² Irkutsk State University, 664003 Russia

³ Hirosaki University, 036-8561 Japan

E-mail: sinegovsky@api.isu.runnet.ru

Abstract. The prompt muon contribution to the deep-sea atmospheric muon flux can serve as a tool for probing into the small- x feature of the gluon density inside of a nucleon, if the muon energy threshold could be lifted to 100 TeV. The prompt muon flux underwater is calculated taking into consideration predictions of recent charm production models in which the small- x behaviour of the gluon distribution is probed. We discuss the possibility of distinguishing the PQCD models of the charm production differing in the small- x exponent of the gluon distribution, in measurements of the muon flux at energies 10100 TeV with neutrino telescopes.

Submitted to: *J. Phys. G: Nucl. Phys.*

1. Introduction

A correct treatment of the charm hadroproduction is important to the atmospheric muon and neutrino studies, since short-lived charmed particles, D^\pm , D^0 , \overline{D}^0 , D_s^\pm , Λ_c^+ , which are produced in collisions of cosmic rays with nuclei of the air, become the dominant source of atmospheric muons and neutrinos at energies $E \sim 100$ TeV. Thus, one needs to take them into consideration as the background for extraterrestrial neutrinos (for a review, see [1]). Muons originating from decay of these charmed hadrons are so called prompt muons (PM) that contribute to the total atmospheric muon flux.

Another aspect of the interest to the charm production relates to the gluon density at small gluon momentum fraction x . The gluon density at small x is of considerable importance because this strongly influences the charm production cross section, both total and inclusive. Recently Pasquali et al. [2] and Gelmini et al. [3, 4] have analysed the influence of small- x behaviour of the parton distribution functions (PDFs) on the atmospheric lepton fluxes at sea level. Based on next-to-leading order (NLO) calculations of the perturbative Quantum Chromodynamics (PQCD), they predict PM

fluxes at the ground level depending strongly on proton gluon distributions at small x scale, $x < 10^{-5}$.

The muon spectra underwater computed with the model of Pasquali et al. [2], in which were used the MRSD₊ [5] and the CTEQ3M [6] sets of PDFs, were recently discussed [7, 8, 9]. In this note, using predictions of the PQCD model [3, 4] for the charm production, we discuss the PM contribution to the deep-sea muon flux at depths typical for operating and constructing neutrino telescopes, AMANDA [10], ANTARES [11], Baikal [12], NESTOR [13]. Due to large detector volume and effective area ($10^4 - 10^5$ m²) and homogeneity of surrounding matter these underice and deep-sea installations have considerable advantages over underground detectors for probing very high-energy atmospheric muons.

Namely, here we try to study a PM flux underwater dependence on the power λ of the small- x gluon distribution function: $xg(x, Q^2) \propto x^{-\lambda}$. The nature of the small- x behaviour of the gluon density is now under extensive discussion (see, for example, [14, 15, 16, 17, 18, 19]). The small- x behaviour of the PDFs is the subject of the deep interest because an understanding of the underlying dynamics is far yet from being clear.

2. PDFs and charm production models

Due to dominant subprocess in heavy quarks hadroproduction, $gg \rightarrow c\bar{c}$, the charm production is sensitive to the gluon density at small x , where x is the gluon momentum fraction. One may evaluate the scale of x in cosmic ray interactions as follows. The product of the gluon momentum fraction x_1 of the projectile nucleon and that of the target x near the charm production threshold ($\sim 2m_c$) is $x_1x = 4m_c^2/(2m_N E_0)$, where E_0 is the primary nucleon energy in the lab frame. Since a muon takes away about 5% of the primary nucleon energy, $E_0 \simeq 20E_\mu$, we have $x_1x = 0.1(m_c/m_N)(m_c/E_\mu)$. Because of the steepness of the primary cosmic ray spectrum only large x_1 contribute sizeably to the atmospheric charm production, so one needs to adopt $x_1 \gtrsim 0.1$. Taking $m_c^2 \simeq 2$ GeV², one may find the range of importance for $E_\mu \gtrsim 100$ TeV to be $x \lesssim 2 \cdot 10^{-6}$. It should be stressed, this range is yet outside of the scope of the perturbative next-to-leading order global analysis of parton distributions [20, 21].

The exponent λ in PQCD charm production models [2, 3, 4] covers wide range from about 0.5, the value being formerly connected to the Pomeron intercept Δ in the leading order of the Balitsky-Fadin-Kuraev-Lipatov (BFKL) approach [22], to about 0.1–0.2 ($\Delta = 0.13 - 0.18$), values obtained with the NLO corrections [23] to the BFKL scheme. The interactions between Pomerons lead to the increase of the BFKL Pomeron intercept [16].

Figure 1 presents the sea-level muon flux measured near the vertical [24, 25, 26, 27, 28, 29], as well as fluxes calculated with taking into account the prompt muon contribution. These ones are predictions of the quark-gluon string model (QGSM) [30, 31] (the dash-dotted line) and the recombination quark-parton model (RQPM) [31, 32] (dashed), as well those of a set of PQCD charm production models by

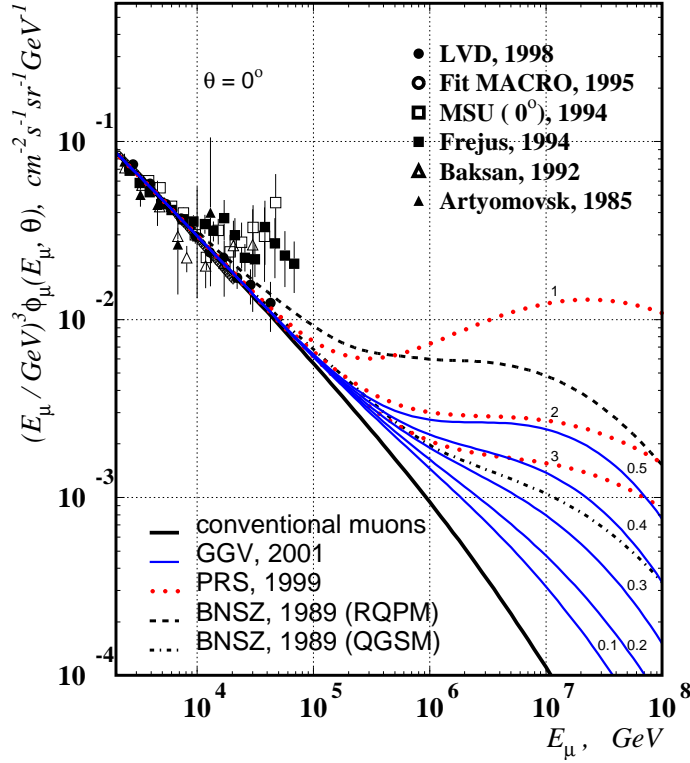


Figure 1. Vertical sea-level muon flux data and predictions. Experiments: \blacktriangle – Artyomovsk [24], \triangle – Baksan [25], \square – MSU [26], \blacksquare – Frejus [27], \circ – MACRO [28], \bullet – LVD [29]. The lower solid line stands for conventional muons. The rest of curves represent the total muon flux, sum of prompt muons and conventional ones.

Pasquali, Reno and Sarcevic [2] (hereafter PRS – dotted lines with numbers 1, 2, 3) and models by Gelmini, Gondolo and Varieschi [3, 4] (GGV – thin curves with numbers 0.1 – 0.5). These models are used further in calculations of the deep-sea muon flux. Let us sketch out PQCD models.

2.1. The model by Pasquali, Reno and Sarcevic

2.1.1. PRS-1. The PRS-1 model (dotted lines in figures 1, 2) (identical with the PQCD-1 in reference [9]) is based on the MRSD₊ set [5]. The PDF input parameters are the followings: $xg(x, Q_0^2) \sim x^{-0.5}$ as $x \rightarrow 0$, 4-momentum transfer squared $Q_0^2 = 4 \text{ GeV}^2$; the sea light quark asymmetry, $\bar{u} < \bar{d}$, is taking into consideration; the QCD scale in the minimal subtraction scheme ($\overline{\text{MS}}$), $\Lambda_4^{\overline{\text{MS}}} = 0.215 \text{ GeV}$, corresponds to the effective coupling at the Z boson mass scale $\alpha_s(M_Z^2) = 0.111$. The factorization scale is $\mu_F = 2m_c$, the renormalization one is $\mu_R = m_c$, where the charm quark mass, m_c , is chosen to be equal 1.3. The sea-level prompt muon flux has been parameterized by authors [2] with the equation:

$$\lg[E_\mu^3 \phi_\mu^{D, \Lambda_c}(E_\mu) \cdot (\text{cm}^{-2} \text{s}^{-1} \text{sr}^{-1} \text{GeV}^2)^{-1}] = -5.91 + 0.290y + 0.143y^2 - 0.0147y^3, \quad (1)$$

where $y = \lg(\frac{E_\mu}{1 \text{ GeV}})$.

2.1.2. PRS-2. In the PRS-2 model (the same as the PQCD-2 in reference [9]) CTEQ3M set [6] was used. Corresponding inputs which were utilized in this model are $\Lambda_4^{\overline{MS}} = 0.239$ GeV, $\alpha_s(M_Z^2) = 0.112$, $m_c = 1.3$ GeV, $\mu_F = 2m_c$, $\mu_R = m_c$, and $\lambda = 0.286$ at $Q_0^2 = 1.6$ GeV. The corresponding approximate expression for the PM spectrum is

$$\lg[E_\mu^3 \phi_\mu^{D, \Lambda_c}(E_\mu) \cdot (\text{cm}^{-2}\text{s}^{-1}\text{sr}^{-1}\text{GeV}^2)^{-1}] = -5.79 + 0.345y + 0.105y^2 - 0.0127y^3. \quad (2)$$

2.1.3. PRS-3. In this model the CTEQ3M set was also used. Differing from PRS-2 in the renormalization and factorization scales, $\mu_F = \mu_R = m_c$, this model shows the uncertainty relating to the scale choice. In this case the PM spectrum was given as

$$\lg[E_\mu^3 \phi_\mu^{D, \Lambda_c}(E_\mu) \cdot (\text{cm}^{-2}\text{s}^{-1}\text{sr}^{-1}\text{GeV}^2)^{-1}] = -5.37 + 0.0191y + 0.156y^2 - 0.0153y^3. \quad (3)$$

2.2. The model by Gelmini, Gondolo and Varieschi

Here we present results for the model, among those discussed in [4], which is based on MRST set of PDFs [20] with different values of the exponent λ in the range $0.1 - 0.5$, $Q^2 \geq 1.25$ GeV²; $\alpha_s(M_Z^2) = 0.1175$. The factorization and renormalization scales are:

$$\mu_F = 2m_T, \mu_R = m_T,$$

where

$$m_T = (k_T^2 + m_c^2)^{1/2}, m_c = 1.25 \text{ GeV},$$

and characteristic transverse momentum k_T is of $\sim m_c$.

In order to compute PM flux underwater we parameterize sea-level muon spectra of the GGV model (see figure 7 in reference [4]) with the formulae:

$$\phi_\mu^{D, \Lambda_c}(E_\mu) = A \left(\frac{E_\mu}{1 \text{ GeV}} \right)^{-(\gamma_0 + \gamma_1 y + \gamma_2 y^2 + \gamma_3 y^3)} \text{cm}^{-2}\text{s}^{-1}\text{sr}^{-1}\text{GeV}^{-1}. \quad (4)$$

In table 1 five sets of the parameters to equation (4) are presented for different values of the index λ of the small- x gluon distribution.

Table 1. Parameters of the prompt muon spectrum at sea level (4).

λ	$A, 10^{-6}$	γ_0	γ_1	$\gamma_2, 10^{-2}$	$\gamma_3, 10^{-3}$
0.1	3.12	2.70	-0.095	1.49	-0.2148
0.2	3.54	2.71	-0.082	1.12	-0.0285
0.3	1.80	2.38	0.045	-0.82	0.911
0.4	0.97	2.09	0.160	-2.57	1.749
0.5	0.58	1.84	0.257	-4.05	2.455

3. The conventional muon flux

The main source of the atmospheric muons up to ~ 50 TeV are decays of secondary cosmic ray pions and kaons. The flux (conventional) of (π, K) -muons is computed based on the nuclear cascade model by [33] (see also [32, 34]). High-energy part of this spectrum for the vertical may be approximated with the equation (in $\text{cm}^{-2}\text{s}^{-1}\text{sr}^{-1}\text{GeV}^{-1}$):

$$\phi_{\mu}^{\pi,K}(E_{\mu}, 0^{\circ}) = \begin{cases} 14.35 E_{\mu}^{-3.672} & \text{for } E_1 < E_{\mu} \leq E_2, \\ 10^3 E_{\mu}^{-4} & \text{for } E_{\mu} > E_2 \end{cases}. \quad (5)$$

where $E_1 = 1.5878 \times 10^3 \text{ GeV}$, $E_2 = 4.1625 \times 10^5 \text{ GeV}$.

Zenith-angle distribution of atmospheric muons at sea-level was computed in the reference [35] where detail comparison between the calculated atmospheric muon spectra and the sea-level experimental data at different zenith angles was made (see also [9]). The conventional muon flux computed for the vertical direction is shown in figure 1 (the lower solid line).

Each of five thin lines in figure 1 presents the sum of the conventional muon flux (5) and the GGV prompt muon flux (4) corresponding to the exponent $\lambda = 0.1, 0.2, 0.3, 0.4, 0.5$ (numbers near lines). Dotted lines show the same for PRS models, equations (1-3). For comparison there are also shown contributions due to the quark-gluon string model and the recombination quark-parton one [31, 32] (the dash-dot line and the dash line respectively). Ratios of prompt muon fluxes to the conventional one are shown in figure 2. As one can see, the crossover energy for the PM flux and conventional one covers the wide region from $\sim 150 \text{ TeV}$ to $\sim 3 \text{ PeV}$, that is more than one order of the magnitude.

It is worth to note that old QGSM prediction [31] at high energies is within GGV prompt muon fluxes as well that of RQPM is within PRS results (figures 1, 2).

4. Prompt muon component of the flux underwater

Muon energy spectra and angle distributions of the flux underwater was computed with the method by [36]. The collision integral in the kinetic equation includes the energy loss of muons due to bremsstrahlung, direct e^+e^- pair production and photonuclear interactions. The ionization energy loss and the small- v part of the loss due to e^+e^- pair production ($v < 2 \cdot 10^{-4}$, where v is the fraction of the energy lost by the muon) were treated as continuous ones.

In our calculations of underwater muon fluxes at different zenith angles, we used, as a boundary spectra, PQCD PM fluxes calculated only for the vertical direction at the ground level, supposing the isotropic approximation for prompt muons to be a reliable at least for $10^4 < E_{\mu} < 10^6 \text{ GeV}$ at zenith angles $\theta \lesssim 80^{\circ}$.

The prompt muon fraction of the flux underwater, R_{pm} , defined as ratio of the prompt muon integral spectrum to the conventional one, is presented in figure 3 for the

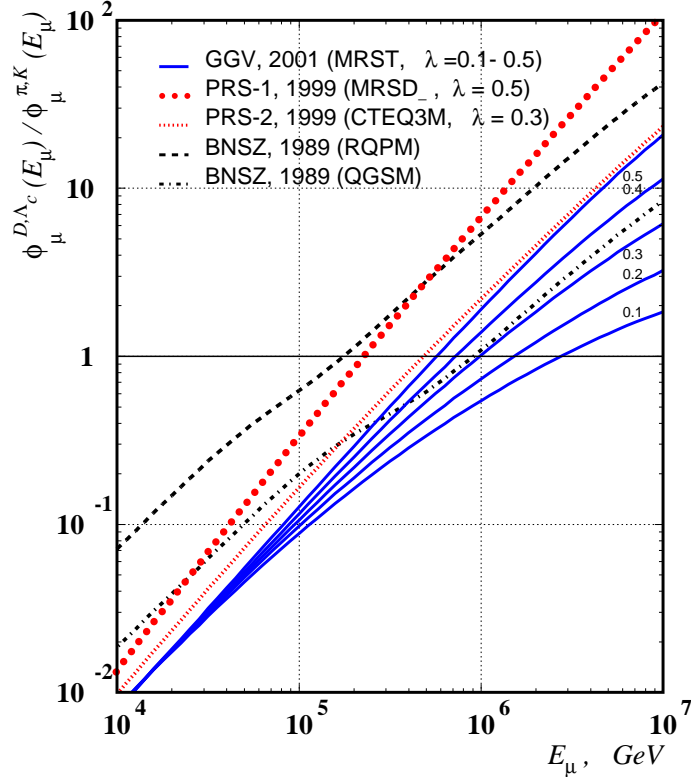


Figure 2. Ratio of the differential prompt muon spectrum at sea level to the conventional one.

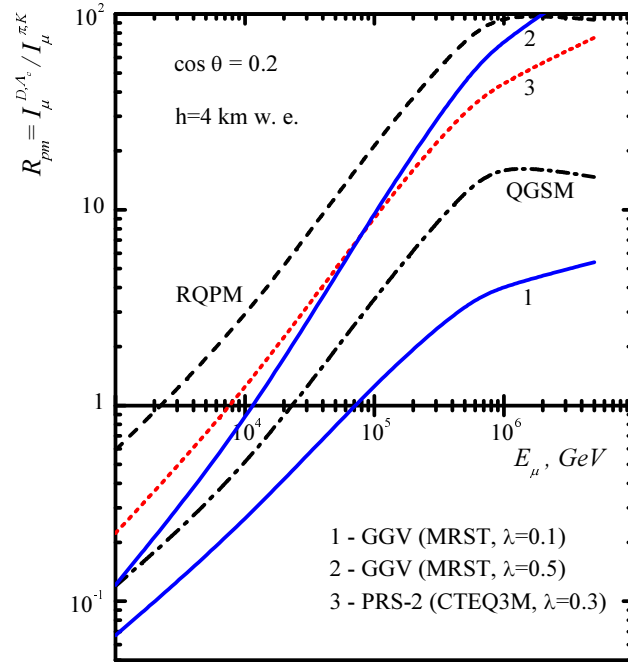


Figure 3. Prompt muon contribution at $h = 4$ km w. e. vs. E_{μ} .

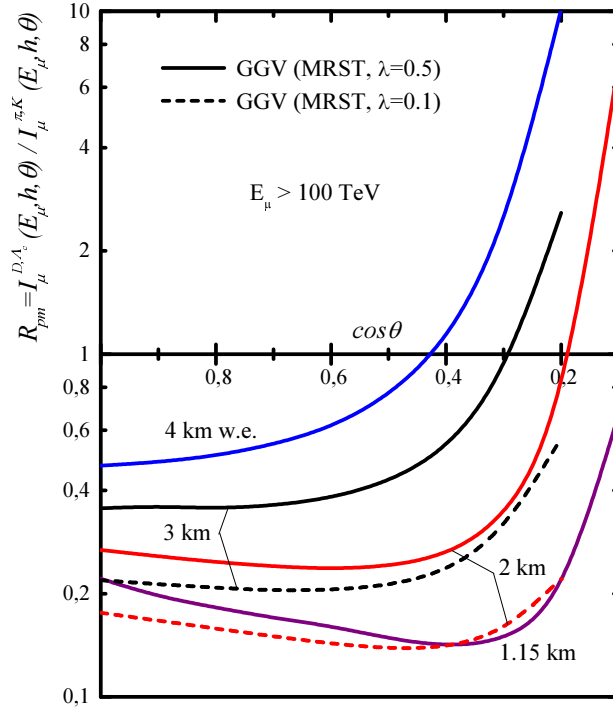


Figure 4. Ratio of the prompt muon flux underwater to the conventional one as a function of $\cos \theta$ at $E_\mu \geq 100$ TeV.

depth of 4 km of the water equivalent (w. e.) and for $\cos \theta = 0.2$. As is seen from this figure, R_{pm} related to the gluon density slope $\lambda = 0.5$ is a factor 3 greater than that for $\lambda = 0.1$ at $E_\mu \gtrsim 10$ TeV.

Zenith-angle distributions of the prompt muon contribution at depths 1-4 km w. e., calculated for $E_\mu > 100$ TeV, are shown in figure 4. Here we used predictions of the GGV model for two values of the gluon density exponent, $\lambda = 0.1$ (dash) and $\lambda = 0.5$ (solid). As one can see in figure 4, R_{pm} increases for the vertical direction from about 0.2 at the depth of the Baikal NT (1.15 km) [12] to about 0.5 at the NESTOR depth (~ 4 km) [13]. For the larger zenith angles, $\theta \sim 75^\circ$, this contribution becomes apparently sizable at depths 3 – 4 km. Differences in the predictions owing to a change of λ , from 0.1 to 0.5 (see $h = 2$ and 3 km w. e.), are also clearly visible: the ratio $R_{pm}(\lambda = 0.5)/R_{pm}(\lambda = 0.1)$ at $h = 2$ km w. e. grows from about 1.5 to about 5 as $\cos \theta$ changes from 1 to 0.2.

Here we supposed no differences between PRS and GGV calculations apart from those related to the charm production cross sections. Actually one needs to compare the primary spectrum and composition, nucleon and meson production cross sections and other details of the atmospheric nuclear cascade being used in above computations. These sources of uncertainties would be considered elsewhere.

5. Summary

In order to test the small- x gluon distribution effect we have computed deep-sea prompt muon fluxes using predictions of charm production models based on NLO calculations of the PQCD [2]-[4]. The possibility to discriminate the PQCD models, differing in the slope of the gluon distribution, seems to be achievable in measurements of the underwater muon flux at energies 50-100 TeV.

Hardly appeared at sea level for energies up to 10^5 GeV (figures 1, 2), a dependence on the spectral index λ of the small- x gluon distribution becomes more distinct at depths 3 – 4 km w. e. (figures 3, 4). At the depth of 4 km and at the angle of $\sim 78^\circ$ one could observe the PM flux to be equal, for $\lambda = 0.5$, to the conventional one even for muon energy ~ 10 TeV (the crossover energy). While for $\lambda = 0.1$ the crossover energy is about 70 TeV. For the high energy threshold, $E_\mu > 100$ TeV, and at $h \lesssim 3$ km w. e., the ratio R_{pm} is nearly isotropic up to $\sim 60^\circ$. The “crossover zenith angle” at a given depth, $\theta_c(h)$, depends apparently on the small- x exponent λ of the gluon density inside colliding nucleons:

$$\cos \theta_c |_{\lambda=0.5} \simeq 0.3 \quad \text{and} \quad \cos \theta_c |_{\lambda=0.1} \simeq 0.1 \quad \text{for } h = 3 \text{ km w. e.}$$

References

- [1] Learned J G and Mannheim K 2000 *Ann. Rev. Nucl. Part. Sci.* **50**, 679.
- [2] Pasquali L, Reno M H and Sarcevic I 1999 *Phys. Rev. D* **59**, 034020.
- [3] Gelmini G, Gondolo P and Varieschi G 2000 *Phys. Rev. D* **61**, 056011.
- [4] Gelmini G, Gondolo P and Varieschi G 2001 *Phys. Rev. D* **63**, 036006.
- [5] Martin A D, Stirling W J and Roberts R G 1993 *Phys. Rev. D* **47**, 867.
- [6] Lai H L et al. 1995 *Phys. Rev. D* **51**, 4763; Lai H L et al. 1997 *Phys. Rev. D* **55**, 1280.
- [7] Misaki A. et al 1999 *Proc. 26 ICRC (Salt Lake City)* vol 2, p 139, hep-ph/9905399.
- [8] Naumov V A, Sinegovskaya T S and Sinegovsky S I 2000 *Phys. Atom. Nucl.* **63**, 1923.
- [9] Sinegovskaya T S and Sinegovsky S I 2001 *Phys. Rev. D* **63**, 096004.
- [10] Andres E et al. (AMANDA Collaboration) 2000 *Astropart. Phys.* **13**, 1.
- [11] Amram P et al. (ANTARES Collaboration) 2000 *Astropart. Phys.* **13**, 127.
- [12] Belolaptikov I A et al. (Baikal Collaboration) 1997 *Astropart. Phys.* **7**, 263.
- [13] Anassontzis E G et al. (NESTOR Collaboration) 2000 *Nucl. Phys. B (Proc. Suppl.)* **85**, 153.
- [14] Andersson B (Small x Collaboration) 2002 Small x phenomenology: Summary and status, hep-ph/0204115.
- [15] Ball R D and Landshoff P V 2000 *J. Phys. G: Nucl. Part. Phys.* **26**, 672.
- [16] Kaidalov A B 2001 Regge poles in QCD, hep-ph/0103011.
- [17] Schleper P 2001 Soft hadronic interactions, hep-ex/0102051.
- [18] Vogt R 2000 *Prog. Part. Nucl. Phys.* **45**, S105.
- [19] Yoshida R (on behalf of ZEUS and H1 Collaboration) 2001 HERA small- x and/or diffraction, hep-ph/0102262.
- [20] Martin A D, Roberts R G, Stirling W J and Torne R S 1999 *Nucl. Phys. B (Proc. Suppl.)* **79**, 105.
- [21] Lai H L et al 2000 *Eur. Phys. J. C* **12**, 375.
- [22] Kuraev E A, Lipatov L N and Fadin V S 1976 *Zh. Eksp. Teor. Fiz.* **71**, 840;
Kuraev E A, Lipatov L N and Fadin V S 1977 *Zh. Eksp. Teor. Fiz.* **72**, 377;
Balitsky I I and Lipatov L N 1978 *Yad. Fiz. Yad. Fiz.* **28**, 1597.
- [23] Brodsky S J et al 1999 *JETP Lett.* **70**, 155, hep-ph/9901229;

- Kim V T, Lipatov L N and Pivovarov G B 1999 The Next-to-Leading dynamics of the BFKL Pomeron, hep-ph/9911242.
- [24] Khalchukov F F et al 1985 *Proc. 19 ICRC (La Jolla)* vol 8, p 12.
- [25] Bakatanov V N et al. 1992 *Yad. Fiz.* **55**, 2107.
- [26] Zatsepin G T et al. Bull. of the Russian Acad. of Sci. Ser. Phys. 1994 **58**, 2050.
- [27] Rhode W 1994 *Nucl. Phys. B* (Proc. Suppl.) **35**, 250.
- [28] Ambrosio M et al (MACRO Collaboration) 1995 *Phys. Rev. D* **52**, 3793.
- [29] Aglietta M et al (LVD Collaboration) 1998 *Phys. Rev. D* **58**, 092005;
Aglietta M et al (LVD Collaboration) 1999 *Phys. Rev. D* **60**, 112001.
- [30] Kaidalov A B 1982 *Phys. Lett. B* **116**, 459;
Kaidalov A B and Piskunova O I 1986 *Sov. J. Nucl. Phys.* **43**, 1545.
- [31] Bugaev E V et al 1989 *Nuovo Cimento C* **12**, 41.
- [32] Bugaev E V et al 1998 *Phys. Rev. D* **58**, 054001.
- [33] Vall A N, Naumov V A and Sinegovsky S I 1986 *Sov. J. Nucl. Phys.* 1986 **44**, 806.
- [34] Naumov V A, Sinegovskaya T S and Sinegovsky S I 1998 *Nuovo Cimento A* **111**, 129.
- [35] Sinegovskaya T S 1999 *Proc. Second Baikal School on Fundamental Physics "Interaction of Radiation and Fields with Matter"* (Irkutsk: Irkutsk University Press) vol 2, p 598 (in Russian).
- [36] Naumov V A, Sinegovsky S I and Bugaev E V 1994 *Phys. Atom. Nucl.* **57**, 412; hep-ph/9301263.